TECHNICAL ARTICLE

Green hydrothermal synthesis of CeO$_2$ NWs–reduced graphene oxide hybrid with enhanced photocatalytic activity

K. Huang,[1,2] M. Lei,[1,2,a)] Y.J. Wang,[2] C. Liang,[2] C.X. Ye,[2] X.S. Zhao,[2] Y.F. Li,[2] R. Zhang,[1,2] D.Y. Fan,[2] and Y.G. Wang[2]

[1]State Key Laboratory of Information Photonics and Optical Communications, Beijing University of Posts and Telecommunications, Beijing 100876, People's Republic of China
[2]School of Science, Beijing University of Posts and Telecommunications, Beijing 100876, People's Republic of China

In this study, CeO$_2$ nanowires–reduced graphene oxide hybrids (CeO$_2$ NWs–RGO) were synthesized by a green hydrothermal method using CeO$_2$ NWs and graphene oxide (GO) as raw materials. During the process of reduction of GO, hydrothermal condition with supercritical water provides thermal and chemical factors to synthesize RGO. The photocatalytic experimental results show that the CeO$_2$ NWs–RGO hybrids exhibit enhanced photocatalytic activity for degradation of Rhodamine B (RhB) under UV-light irradiation. It is found that the degree of photocatalytic activity enhancement strongly depends on the mass ratio of RGO in the hybrids, and the remarkable photocatalytic activity is 20 times that of pristine CeO$_2$ NWs when the loading amount of RGO is 8.0 wt%. The enhancement of photocatalytic activity can be attributed to the excellently elevated absorption ability for the dye through π–π conjugation as well as the effective inhibition of the recombination of photogenerated electrons because of the electronic interaction between CeO$_2$ NWs and RGO sheets. © 2014 International Centre for Diffraction Data. [doi:10.1017/S0885715613000663]

Key words: Green hydrothermal method, CeO$_2$ NWs, reduced graphene oxide, photocatalysis

I. INTRODUCTION

Recently, Graphene-based hybrids have attracted much attention in the materials research field because of their great usefulness in electronics (Kim *et al.*, 2009), photocatalysis (Zhang *et al.*, 2010), and photovoltaic devices (Kamat, 2010). As a one-atom-thick and two-dimensional honeycomb lattice structure, graphene has high specific surface area and remarkable electrical (Wang *et al.*, 2010), thermal (Si and Samulski, 2008), optical and mechanical properties (Lee *et al.*, 2010), which makes it a novel material for the preparation of high performance composites with other functional materials. CeO$_2$ as one of the inexpensive and relatively harmless rare earth materials, has been extensively studied for many technological applications such as catalyst (Zhong *et al.*, 2007), fuel, or solar cell (Corma *et al.*, 2004; Deluga *et al.*, 2004), sensor (Liao *et al.*, 2008), luminescent and UV shielding (Wang *et al.*, 2011). Moreover, CeO$_2$ can be considered as an n-type semiconductor with a wide band gap of 2.9–3.2 eV, and it has some properties similar to commonly used photocatalyst TiO$_2$ such as nontoxicity, high stability, and strong absorption in the UV region (Ji *et al.*, 2009). Thus, CeO$_2$ can be regarded as a potential photocatalyst for hydrogen gas generation by splitting water and photodegradation of organic pollutants. However, It has been reported that CeO$_2$ exhibits a relatively low photocatalytic activity for the oxidation of pollutants in water compared with TiO$_2$ under UV irradiation (Khalil *et al.*, 1998; Subramanian *et al.*, 2001;

Miyauchi *et al.*, 2002). Moreover, Mauro *et al.* (2012) have successfully synthesized CeO$_2$–graphene composite using a two-step route and this composite has also shown remarkable thermal stability up to 1400 °C. Zhang *et al.* (2013) have also developed a CeO$_2$–graphene composites-based ECL biosensor for detection of cholesterol, which shows outstanding reproducibility, long-term stability, and selectivity. Ling *et al.* (2013) have reported a facile synthesis of layered CeO$_2$–graphene hybrid with superior catalytic performance in dehydrogenation of ethylbenzene. Here, we developed a novel CeO$_2$ nanowires–reduced graphene oxide (CeO$_2$ NWs–RGO) hybrid photocatalyst through a green and simple hydrothermal process, during which the coupling between graphene oxide (GO) and CeO$_2$ NWs and the subsequent *in situ* reduction of GO to RGO was achieved. The photocatalytic performance and adsorption ability for dyes were also investigated. Furthermore, it is demonstrated that all the CeO$_2$ NWs–RGO hybrids exhibit higher photocatalytic activity than pristine CeO$_2$ NWs because of the improved adsorption ability for dyes and the efficient separation of photogenerated electron/hole pairs by RGO.

II. EXPERIMENTAL

A. Synthesis of CeO$_2$ NWs-RGO hybrid

All of the chemical reagents in this paper were of analytical grade and used as received without further purification. Before the synthesis of CeO$_2$ NWs–RGO hybrids, GO was synthesized from natural graphite powder (99.9%) by the reported method with slight modification (Xu *et al.*, 2008; Pant *et al.*, 2013). CeO$_2$ nanowires (CeO$_2$ NWs) were

synthesized by a typical hydrothermal method according to the previous reported work (Fu *et al.*, 2007) and then annealed at 350 °C for 4 h in order to obtain a clean CeO_2 surface after the removal of surface adsorbed substances. The CeO_2 NWs–RGO hybrids were obtained via a one-step hydrothermal method using supercritical water as green reductant. Briefly, 0.2 g of CeO_2 NWs were first added into the calculated amount of GO solution followed by ultrasonic dispersion for 30 min and vigorous stirring for another 2 h to disperse CeO_2 NWs sufficiently. Then, the mixing solution was transferred into a 50 ml Teflon-sealed autoclave at 150 °C for 5 h and cooled down to room temperature naturally. The resulting hybrids were recovered by centrifugation, washed with DI water and alcohol several times, and fully dried in vacuum at 60 °C for 12 h. The amount of graphene in the CeO_2 NWs–RGO hybrid was controlled to be 0, 0.5, 1.0, 2.0, 4.0, 6.0, and 8.0 wt%, and the corresponding samples were labeled as CG-0, CG-0.5, CG-1.0, CG-2.0, CG-4.0, CG-6.0, CG-8.0, and CG-10.0, respectively.

B. Photocatalytic activity measurements

The evaluation of photocatalytic activity of the prepared samples for photocatalytic decomposition of Rhodamine B (RhB) dyes was performed at room temperature and observed based on the absorption spectroscopic technique. Typically, 100 ml aqueous solution of RhB dyes (4.79 g l^{-1}) and 50-mg as-prepared samples were dispersed in a 200-ml breaker. Then, the mixture was kept in the dark under stirring for 1 h to evaluate the dyes adsorptivity of various samples before the photocatalytic reaction was started by exposing the vessel under the UV irradiation (produced by a 500 W long arc mercury lamp with the main wave crest at 365 nm and intensity at the mixture surface was 25 W cm^{-2}). At given time intervals of 15 min, 3 ml aliquots were sampled, at once, centrifuged at 4000 rpm for 5 min to deposit the as-prepared photocatalysts during both stages of dark stirring and UV irradiation.

C. Characterization

X-ray diffraction (XRD) patterns were obtained on an X'pert PRO x-ray diffractometer (PANalytical, The Netherlands) with Cu $K\alpha$ as radiation source ($\lambda = 0.154\,06$ nm). Morphological analysis was performed with an S-4800 field emission scanning electron microscope (FESEM, Hitachi, Japan) with an acceleration voltage of 10 kV. UV–vis absorption spectra were acquired using a UV–visible spectrophotometer (UV-2800, Shanghai Sunny Hengping Scientific Instrument Co., LTD) and the irradiation intensity was estimated with a radiometer, Model: UV-A, made in Photoelectric Instrument Factory of Beijing Normal University. UV–vis absorption spectra were acquired using a UV–Vis spectrophotometer (Varian Cary 5000, USA).

III. RESULTS AND DISCUSSION

As shown in Figure 1(a), the synthesis mechanism of CeO_2 NWs–RGO hybrids can be interpreted as follows. The presence of oxygen-containing functional groups in GO provides the opportunities to attach the one-dimensional metal oxide nanostructure and facilitates the initial formation of coupling between GO and CeO_2 NWs, as reported by Zhou

et al. (2012) and Nguyen-Phan *et al.* (2012). With increasing temperature and pressure, supercritical water can exhibit strong reducing power during the hydrothermal process, resulting in the cleavage reactions of various heterolytic bonds on the surface of GO, which is similar to the preparation of carbon-based nanostructures via the deoxygenation reaction of carbohydrates by Yao *et al.* (2007) and Sun and Li (2004). It is clear that the GO shows a characteristic diffraction peak at $2\theta = 11.3°$ [Figure (2i)] whereas two broad peaks at 22.7 and 42.8° are observed after the hydrothermal process, which can be ascribed to RGO (002) and (100) planes (Ahmad *et al.*, 2013), suggesting that GO sheet is effectively reduced to RGO though the green hydrothermal treatment. As for the CeO_2 NWs–RGO hybrid, most of the diffraction peaks can be indexed to the fluorite cubic phase of CeO_2 (JCPDF No. 65-2975) with lattice constants $a = 0.5411$ nm and average crystalline size of 14 nm as calculated by the Scherrer formula, and it is clear that there is a visible cover of RGO sheets on the surface of CeO_2 NWs [Figure (3c)]. However, no characteristic diffraction peaks corresponding to RGO can be observed [Figures 2(a)–2(g)], which is because of the limited amount and the destroyed regular stacks of RGO in the hybrids as proposed by Li *et al.* (2011). In addition, the morphology of the synthesized CeO_2 NWs can be obviously characterized with the average diameter of about 30–80 nm and the length of several micrometers, as shown in Figure 3(b).

The photocatalytic activity of the CeO_2 NWs and CeO_2 NWs–RGO hybrids was evaluated by the photocatalytic decomposition of RhB aqueous solution under UV-light irradiation. It is well known that the photocatalytic decomposition of organic dyes usually takes place on the surface of a photocatalyst, sufficient contact between organic dyes and photocatalysts is an key factor for achieving higher photocatalytic performance (Wang *et al.*, 2012), the adsorption ability for RhB dyes of various samples was investigated before UV-light irradiation to further illustrate the photocatalytic mechanism of CeO_2 NWs–RGO hybrids, as shown in Figures 1(b) and 4. It is notable that the adsorption ability for RhB is significantly improved with increasing amount of RGO in the CeO_2 NWs–RGO hybrids and the absorptance of CG-10.0 are as high as 89% (Figure 5), suggesting the feasible transfer for dyes molecules from the solution to the surface of the photocatalyst via the π–π conjugation between RhB dyes and RGO nanosheets (Perera *et al.*, 2012).

As for the photodecomposition of RhB dyes, the photocatalytic degradation reaction can be assumed to follow a pseudo-first-order expression: $\ln(C_0/C) = kt$, where C_0/C is the normalized organic compounds concentration and k is the apparent reaction rate (min^{-1}), as shown in Figures 5 and 6. It is clear that all the CeO_2 NWs–RGO hybrids exhibit a higher photocatalytic activity than the pure CeO_2 NWs ($k = 0.000\,96$ min^{-1}) and CG-8.0 even shows a highly enhanced photocatalytic performance with a k value of 0.0197 min^{-1}, which is about 20 times that of pure CeO_2 NWs. Moreover, the k values also show an obvious enhancement with the increasing amount of RGO in the CeO_2 NWs–RGO hybrids, and the photoreacted solution of CG-6.0 and CG-8.0 is almost transparent under irradiation for 1 h. However, the photocatalytic activity of CG-10.0 exhibits an obvious decrease compared with that of CG-6.0 and CG-8.0 as shown in Figures 5 and 6, and we attribute this lower activity to the lower excitation efficiency of CeO_2 in the hybrid because of the
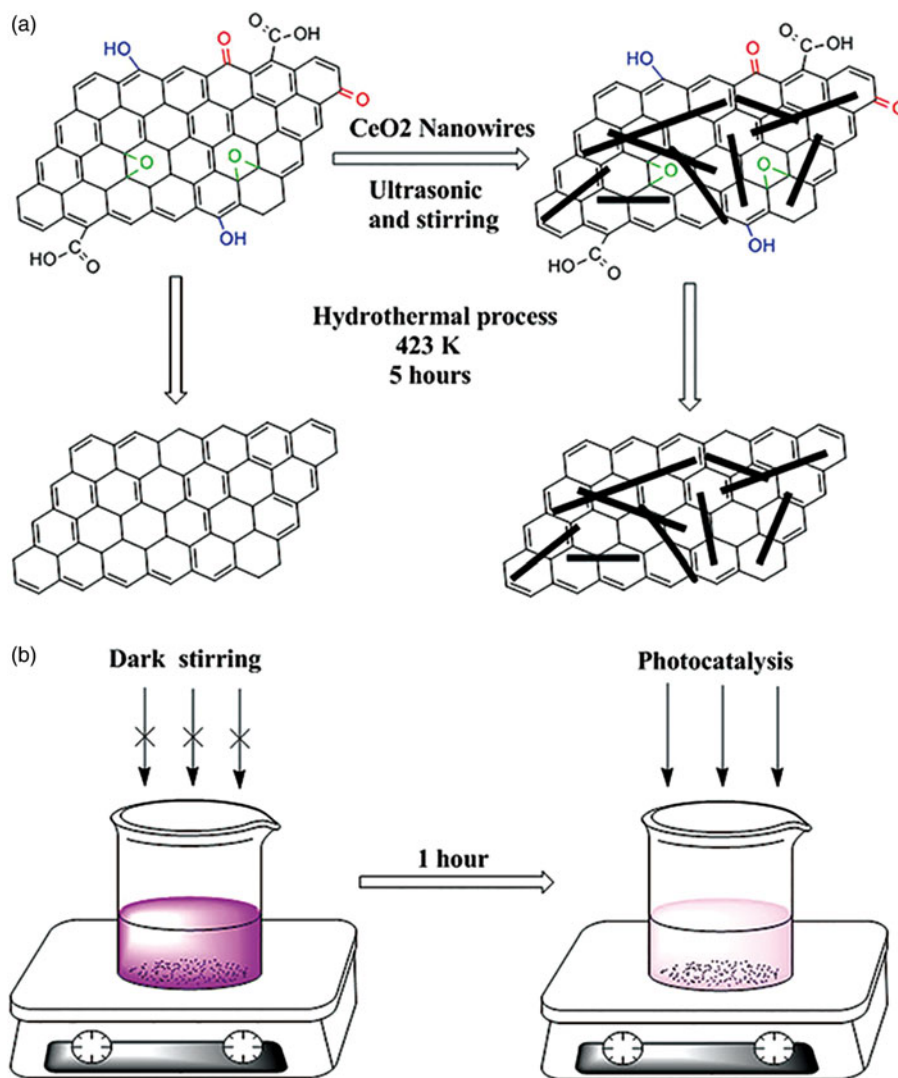
Figure 1. (Color online) Schematic illustration of (a) the formation of RGO–ZnO NRs composites and (b) the measurement of photocatalytic degradation performance for various samples.
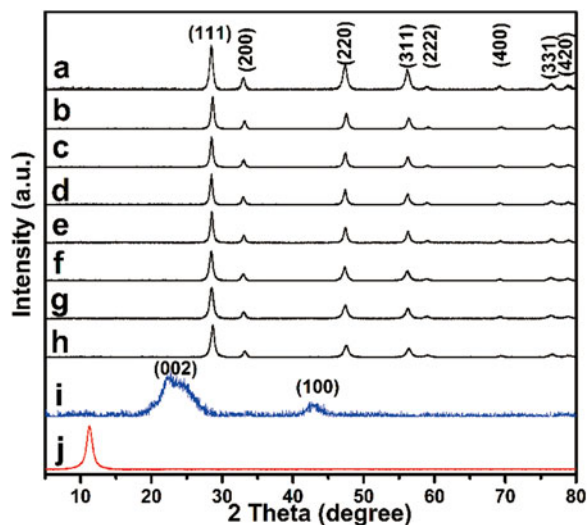

Figure 2. (Color online) XRD Patterns of the (a) CG-0, (b) CG-0.5, (c) CG-1.0, (d) CG-2.0, (e) CG-4.0, (f) CG-6.0, (g) CG-8.0, (h) CG-8.0, (i) RGO, and (j) GO.

increased absorbance or scattering of irradiation through excess RGO in the reaction solution, according to the previous report by Wang and Zhang (2011). To further confirm this reasonable interpretation, the typical UV–vis absorption spectra of various samples are shown in Figure 7. It is noted that all
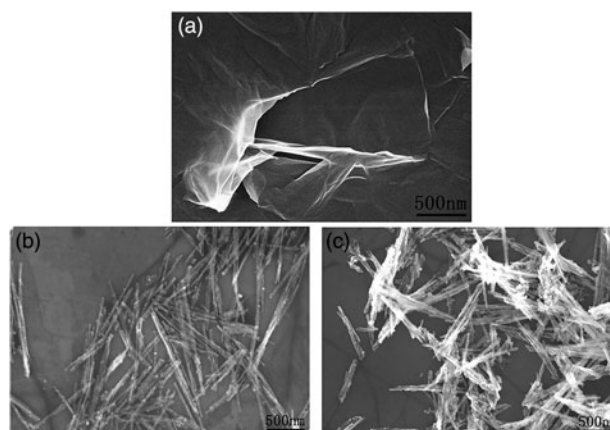

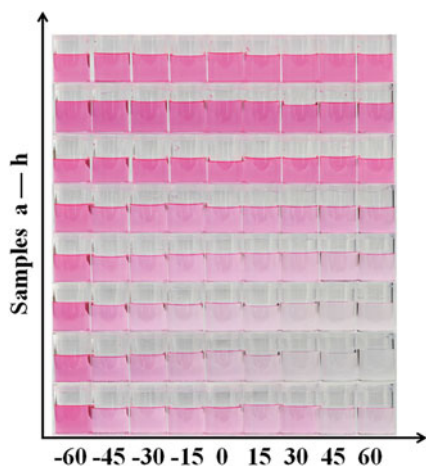Figure 3. FESEM images of the (a) GO, (b) CeO$_2$ NRs, and (c) CG-8.0.

Figure 4. (Color online) Images of the degradation effect for (a) CG-0, (b) CG-0.5, (c) CG-1.0, (d) CG-2.0, (e) CG-4.0, (f) CG-6.0, (g) CG-8.0, and (h) CG-10.0.

Figure 6. (Color online) Photocatalytic activity for RhB degradation under UV-light irradiation of (a) CG-0, (b) CG-0.5, (c) CG-1.0, (d) CG-2.0, (e) CG-10.0, (f) CG-4.0, (g) CG-6.0, and (h) CG-8.0.

of the spectra exhibit a strong absorption below 400 nm with an absorption peak of about 355 nm and the prepared CeO_2 NWs–RGO hybrids show an obviously enhanced adsorption compared with CeO_2 NWs, and the enhancements of absorption increase with RGO contents of the CeO_2 NWs–RGO hybrids, suggesting that the increased absorbance of irradiation through excess RGO really reduces the excitation efficiency of CeO_2 in the hybrid. Moreover, the absorption edge of CeO_2 NWs–RGO hybrids also displays a slight red-shift to higher wavelength with the increase of RGO content, which we attribute to the chemical bonding between CeO_2 and RGO as similar reports obtained for TiO_2–RGO composite materials (Lee *et al.*, 2012).

As per the discussion above, the enhancement of photocatalytic activity can be attributed to the elevated absorption ability for dyes molecules as well as the effect of the effective inhibition of the recombination of photogenerated electron–hole pairs, as shown in Figure 8. Possible major photocatalytic reaction steps can be summarized as follows:
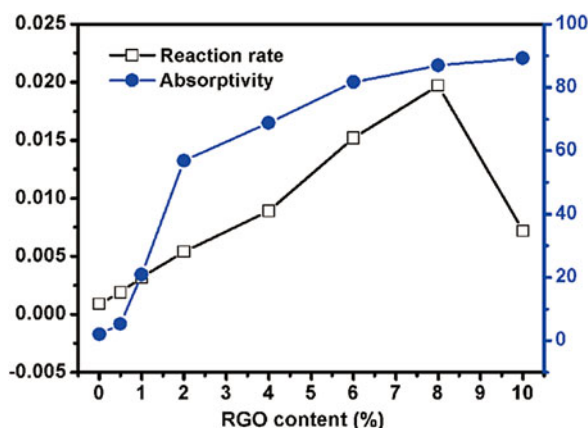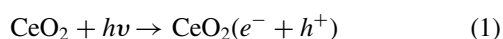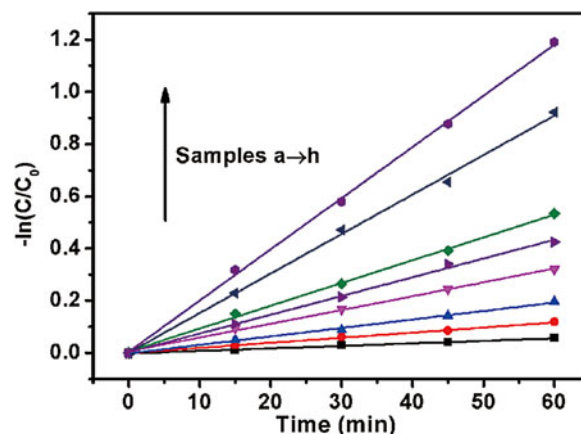
$$CeO_2 + h\upsilon \rightarrow CeO_2(e^- + h^+) \tag{1}$$

$$CeO_2(e^-) + RGO \rightarrow CeO_2 + RGO(e^-) \tag{2}$$

$$O_2 + RGO(e^-) \rightarrow RGO + O_2^- \tag{3}$$

$$Dyes + RGO \rightarrow RGO(Dyes) \tag{4}$$

$$CeO_2(e^-) + RGO(Dyes) \rightarrow CeO_2 + RGO + OX\text{Prod.} \tag{5}$$

$$O_2^- + RGO(Dyes) \rightarrow RGO + OX\text{Prod.} \tag{6}$$

Photogenerated electrons can quickly transfer to the RGO nanosheets and then react with the ubiquitously dissolved oxygen molecule to yield reactive oxygen species. In this case, the RGO nanosheets function as an effective cocatalyst and an electron sink to accept photogenerated electrons from excited CeO_2 NWs, resulting in a rapid transfer of photogenerated electrons and thus a lower recombination rate of photogenerated electron/hole pairs. Meanwhile, the resultant hole in the valence band of CeO_2 NWs can decompose the RhB dyes by direct oxidation because of the sufficient adsorbance of RhB dyes molecules on the surface of RGO and the strong coupling of CeO_2 NWs and RGO, which has been demonstrated by Xu *et al.* (2011). Furthermore, once the RhB dyes molecules adsorbed on the surface of RGO are degraded, the RhB dyes molecules in solution can immediately diffuse onto the surface of RGO via the π–π conjugation to be further decomposed.

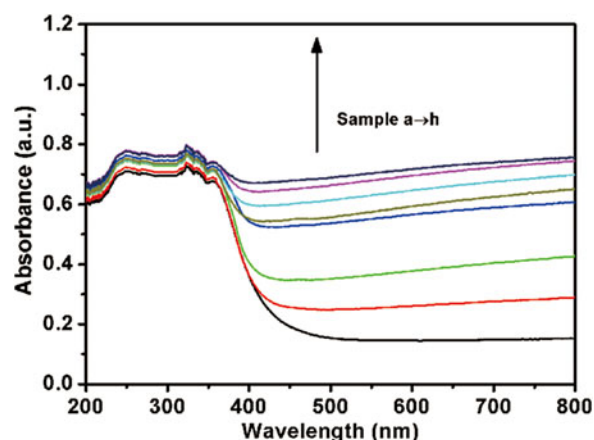Figure 5. (Color online) Reaction rate k and dye absorptivity of various samples.

Figure 7. (Color online) UV-vis absorption spectra of (a) CG-0, (b) CG-0.5, (c) CG-1.0, (d) CG-2.0, (e) CG-4.0, (f) CG-6.0, (g) CG-8.0, and (h) CG-10.0.
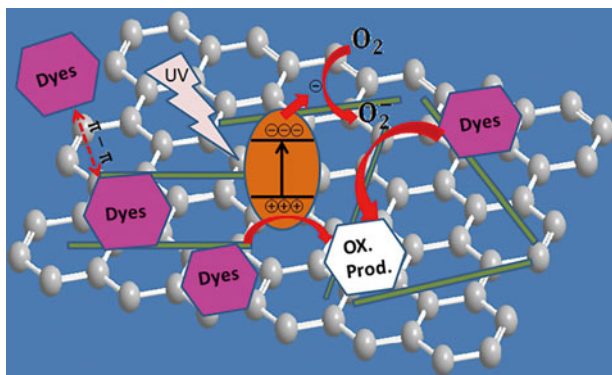
Figure 8. (Color online) Photocatalytic degradation mechanism for dyes over CeO_2 NWs–RGO hybrids under UV-light irradiation.

IV. CONCLUSION

In summary, CeO_2 NWs–RGO hybrids with different RGO content were successfully synthesized by a green hydrothermal method without using any additive and surfactant. The possible formation mechanism can be attributed to the initial binding of the CeO_2 NWs with GO sheets through carboxyl and oxygen linkages and subsequent *in situ* reduction of GO to RGO by supercritical water during hydrothermal process. Owing to the introduction of RGO, both the adsorption ability for dyes and the separation ratio of photogenerated electron–hole pairs have been greatly enhanced. The photodegradation results demonstrate that the content of RGO in hybrids has a great influence on the photocatalytic activity, obviously increased to almost 20 times when loaded with 8.0 wt% of RGO. This work has demonstrated that the novel CeO_2–graphene hybrid can be used as an alternate photocatalyst for water environment protection.

Ahmad, M., Ahmed, E., Hong, Z. L., Xu, J. F., Khalid, N. R., Elhissi, A., and Ahmed, W. (**2013**). "A facile one-step approach to synthesizing ZnO/graphene composites for enhanced degradation of methylene blue under wisible light," Appl. Surf. Sci. **274**, 273–281.

Corma, A., Atienzar, P., Garcia, H., and Chane-Ching, J. Y. (**2004**). "Hierarchically mesostructured doped CeO2 with potential for Solar-Cell use," Nat. Mater. **3**, 394–397.

Deluga, G. A., Salge, J. R., Schmidt, L. D., and Verykios, X. E. (**2004**). "Renewable hydrogen from ethanol by autothermal reforming," Science **303**, 993–997.

Fu, X. Q., Wang, C., Yu, H. C., Wang, Y. G., and Wang, T. H. (**2007**). "Fast humidity sensors based on CeO_2 nanowires," Nanotechnology **18**, 145503.

Ji, P. F., Zhang, J. L., Chen, F., and Anpo, M. (**2009**). "Study of adsorption and degradation of acid Orange 7 on the surface of CeO_2 under visible light irradiation," Appl. Catal. B, Environ. **85**, 148–154.

Kamat, P. V. (**2010**). "Graphene-based nanoarchitectures. Anchoring semiconductor and metal nanoparticles on a two-dimensional carbon support," J. Phys. Chem. Lett. **1**, 520–527.

Khalil, L. B., Mourad, W. E., and Rophael, M. W. (**1998**). "Photo-catalytic reduction of environmental pollutant Cr (VI) over some semiconductors under UV/visible light Illumination," Appl. Catal. B, Environ. **17**, 267–273.

Kim, S. R., Parvez, M. K., and Chhowalla, M. (**2009**). "UV-reduction of graphene oxide and its application as an interfacial layer to reduce the black-transport reactions in dye-sensitized solar cells," Chem. Phys. Lett. **483**, 124–127.

Lee, D. H., Kim, J. E., Han, T. H., Hwang, J. W., Jeon, S., Choi, S. Y., Hong, S. H., Lee, W. J., Ruoff, R. S., and Kim, S. O. (**2010**). "Versatile carbon hybrid films composed of vertical carbon nanotubes grown on mechanically compliant graphene films," Adv. Mater. **22**, 1247–1252.

Lee, J. S., You, K. H., and Park, C. B. (**2012**). "Low bandgap TiO2 nanoparticles wrapped by graphene," Adv. Mater. **24**, 1084–1088.

Li, Q., Guo, B. D., Yu, J. G., Ran, J. R., Zhang, B. H., Yan, H. J., and Gong, J. R. (**2011**). "Highly efficient visible-light-driven photocatalytic hydrogen production of CdS-cluster-decorated graphene nanosheets," J. Am. Chem. Soc. **133**, 10878–10884.

Liao, L., Mai, H. X., Yuan, Q., Lu, H. B., Li, J. C., Liu, C., Yan, C. H., Shen, Z. X., and Yu, T. (**2008**). "Single CeO_2 nanowire gas sensor supported with Pt nanocrystals: gas sensitivity, surface bond states, and chemical mechanism," J. Phys. Chem. C **112**, 9061–9065.

Ling, Q., Yang, M., Rao, R. C., Yang, H. X., Zhang, Q. Y., Liu, H. D., and Zhang, A. M. (**2013**). "Simple synthesis of layered CeO_2-graphene hybrid and their superior catalytic performance in dehydrogenation of ethylbenzene," Appl. Surf. Sci. **274**, 131–137.

Mauro, F. P. S., Heloisa, C. J. F. C., Eduardo, R. T., Mario, J. P., and Paulo, C. I. (**2012**). "Synthesisand characterization of CeO_2-graphene composite," J. Therm. Anal. Calorim. **107**, 257–263.

Miyauchi, M., Nakajima, A., Watanabe, T., and Hashi-moto, K. (**2002**). "Photocatalysis and photoinduced hydrophilicity of various metal oxide thin films," Chem. Mater. **14**, 2812–2816.

Nguyen-Phan, T., Pham, V. H., Kweon, H., Chung, J. S., Kim, E. J., Hur, S. H., and Shin, E. W. (**2012**). "Uniform distribution of TiO2 nanocrystals on reduced graphene oxide sheets by the chelating ligands," J. Colloid Interface Sci. **367**, 139–147.

Pant, H. R., Park, C. H., Pokharel, P., Tijing, L. D., Lee, D. S., and Kim, C. S. (**2013**). "ZnO micro-flowers assembled on reduced graphene sheets with high photocatalytic activity for removal of pollutants," Power today **235**, 853–858.

Perera, S. D., Mariano, R. G., Vu, K., Nour, N., Seitz, O., Chabal, Y., and Balkus, K. J., Jr. (**2012**). "Hydrothermal synthesis of graphene-TiO2 nanotube composites with enhanced photocatalytic actibity," ACS Catal. **2**, 949–956.

Si, Y. and Samulski, E. T. (**2008**). "Exfoliated graphene separated by platinum nanoparticles," Chem. Mater. **20**, 6792–6797.

Subramanian, V., Wolf, E., and Kamat, P. V. (**2001**). "Semiconductor-metal composite nanostructures. to what extent do metal nanoparticles improve the photocatalytic activity of TiO2 Films," J. Phys. Chem. B **105**, 11439–11446.

Sun, X. M., and Li, Y. D. (**2004**). "Colloidal carbon spheres and their core/shell structures with noble-metal nanoparticles," Angew. Chem. Int. Edit. **43**, 597–601.

Wang, F. and Zhang, K. (**2011**). "Reduced graphene oxide-TiO2 nanocomposite with high photocatalystic activity for the degradation of rhodamine B," J. Mol. Catal. A, Chem. **345**, 101–107.

Wang, H., Robinson, J. T., Diankov, G., and Dai, H. (**2010**). "Nanocrystal growth on graphene with various degrees of oxidation," J. Am. Chem. Soc. **132**, 3270–3271.

Wang, Z. L., Li, G. R., Ou, Y. L., Feng, Z. P., Qu, D. L., and Tong, Y. X. (**2011**). "Electrochemical deposition of Eu^{3+}-doped CeO_2 nanobelts with enhanced optical properties," J. Phys. Chem. C **115**, 351–356.

Wang, W. G., Yu, J. G., Xiang, Q. J., and Cheng, B. (**2012**). "Enhanced photocatalytic activity of hierarchical macro/mesoporous TiO2-graphene composites for photodegradation of acetone in air," Appl. Catal. B, Environ. **119**, 109–116.

Xu, Y., Bai, H., Lu, G. W., Li, C., and Shi, G. Q. (**2008**). "Flexible graphene films via the filtration of water-soluble noncovalent functionalized graphene sheets," J. Am. Chem. Soc. **130**, 5856–5857.

Xu, T. G., Zhang, L. W., Chen, H. Y., and Zhu, Y. F. (**2011**). "Significantly enhanced photocatlytic performance of ZnO via graphene hybridization and the mechanism study," Appl. Catal. B, Environ. **101**, 382–387.

Yao, C. H., Shin, Y. S., Wang, L. Q., Windisch, C. F. Jr., Samuels, W. D., Arey, B. W., Wang, C. M., Risen, W. M. Jr., and Exarhos, G. J. (**2007**). "Hydrothermal dehydration of aqueous fructose solutions in a closed system," J. Phys. Chem. C **111**, 15141–15145.

Zhang, H., Lv, X. J., Li, Y. M., Wang, Y., and Li, J. H. (**2010**). "P25-graphene composite as a high performance photocatalyst," ACS Nano **4**, 380–386.

Zhang, M. H., Yuan, R., Chai, Y. Q., Wang, C., and Wu, X. P. (**2013**). "Cerium oxide–grapheme as the matrix for cholesterol sensor," Anal. Biochem. **436**, 69–74.

Zhong, L. S., Hu, J. S., Cao, A. M., Liu, Q., Song, W. G., and Wan, L. J. (**2007**). "3D flowerlike ceria micro/nanocomposite structure and its application for water treatment and CO removal," Chem. Mater. **19**, 1648–1655.

Zhou, X., Shi, T. J., and Zhou, H. O. (**2012**). "Hydrothermal preparation of ZnO-reduced graphene oxide hybrid with high performance in photocatalytic degradation," Appl. Surf. Sci. **258**, 6204–6211.